4858 *Macromolecules* **2009**, *42*, 4858–4866
DOI: 10.1021/ma900605z

Macromolecules
ARTICLE

Fluorescence Correlation Spectroscopy Study of Molecular Probe Diffusion in Polymer Melts

T. Cherdhirankorn,[†] V. Harmandaris,[†,§] A. Juhari,[†] P. Voudouris,[‡] G. Fytas,[†,‡] K. Kremer,[†] and K. Koynov*,[†]

[†]*Max-Planck-Institute of Polymer Research, D-55128 Mainz, Germany,* [‡]*Departments of Chemistry and Materials Science and Technology, University of Crete and FORTH, 71110 Heraklion, Greece, and* [§]*Department of Applied Mathematics, University of Crete, 71110 Heraklion, Greece*

Received December 11, 2008; Revised Manuscript Received May 7, 2009

ABSTRACT: Fluorescence correlation spectroscopy (FCS) was employed to study the diffusion of molecular tracers in different polymer melts (polydimethysiloxane (PDMS), 1,4-*cis*-polyisoprene (PI), poly-(vinylethylene) (PVE), and a symmetric PI/PVE blend) as a function of molecular weight (M_w) and temperature (T). The single molecule sensitivity of the FCS technique precludes any modification of the matrix polymer properties. In all studied systems, the small tracer diffusion coefficient $D(M_w,T)$ senses local segmental dynamics depending on the glass transition temperature $T_g(M_w)$ of the polymer matrix and not its macroscopic viscosity. From the good representation of the $D(T)$ data by the common non-Arrhenius (VFT) function, we found that the activation energy (B_D) increases with tracer size (R) and for a given tracer the value of B_D in PI is almost 2 times bigger than in PDMS. The possibility to establish a direct relation between $D(T)$ and the segmental relaxation time $\tau(T)$ of the polymer matrix was critically addressed based on experimental data in dynamically homogeneous (homopolymers) and heterogeneous (miscible blend) systems and discussed in view of recent computer simulations of polymer/penetrant mixtures.

1. Introduction

The molecular and macromolecular tracer diffusion in undiluted polymer systems has been intensely studied over the past several decades.[1−8] Apart from the fundamental interest, the processes that take place in such systems have also technological importance. The average molecular weight and its distribution, for example, are among the physical properties influenced by the diffusion-controlled termination step of free radical polymerization reactions. In addition, molecular transport of small molecules affects the mixing of plasticizers with polymers, the removal of residual monomer or solvent from polymers through the devolatilization process, and the formation of films, coatings, and foams from the polymer−solvent mixture. Access and control of the local friction in polymer-based systems are very important since it is the main kinetic factor for hierarchical larger scale motions, e.g., self-diffusion. For small molecule diffusion in polymer matrices, breakdown of Debye−Stokes−Einstein (DSE, $D \sim \eta^{-1}$) scaling has been revealed.[3−5,8] Furthermore, it was shown that the probe size, shape, and flexibility significantly affected the magnitude and temperature dependence of translational diffusion coefficients of probes in polymers.[1,3,4]

So far, the diffusion of small molecules in polymer matrices was mostly analyzed by free volume theories[1,9−12] and also discussed in terms of the segmental dynamics of the polymer matrix.[2−7,13] The basic assumption in the free volume theories is that molecular transport relies on a continuous redistribution of free volume elements within the liquid and that the availability of free volume within the system controls the molecular transport.[9] However, such theories are considered to be semiempirical and involve many parameters that are not trivial to obtain in a rigorous way.[11,14] Atomistic molecular dynamics (MD) simulations have the advantage that they provide a detailed molecular representation of the mobility of molecules and have been used extensively in the literature for studying penetrant dynamics in polymer/penetrant systems[14−18] (and references therein). In spite of the extensive theoretical and experimental effort in the past decade, the relationship between molecular probe diffusion and segmental dynamics in polymer melts is still unclear. Whether the polymer segmental dynamics associated with the primary α-relaxation can be deduced from the probe diffusion remains an open question.

Among the several techniques utilized in this endeavor are fluorescence recovery after photobleaching (FRAP),[2,8] fluorescence nonradiative energy transfer (NRET),[3,4] and forced Rayleigh scattering (FRS).[1,7] In the recent years, the fluorescence correlation spectroscopy (FCS) has emerged as a powerful tool for investigation of the diffusion of fluorescent molecules, macromolecules, or nanoparticles in various environments. The method is based on measurement of the fluctuations of the fluorescent light intensity caused by the excursion of fluorescent species through an extremely small observation volume (<1 μm^3) defined by the focus of a confocal microscope.[19] A correlation analysis of these fluctuations yields the diffusion coefficient of the fluorescent species in the broad range $10^{-9}-10^{-15}$ m^2/s. Furthermore, FCS is a single molecule spectroscopic technique free of intermolecular interactions and slow contributions, e.g., clusters, as compared to dynamic light scattering (DLS) and X-ray photon correlation spectroscopy (XPCS), possessing in addition species selectivity. Despite its great potential and high versatility in addressing the diffusion and transport properties in complex systems, so far the utilization of the FCS has been limited mainly to biological, i.e., aqueous environments.[19] Only recently FCS was successfully applied to study the size and conformational changes of macromolecules in organic solvents,[20,21] adsorbed polymers,[22,23] grafted gel,[24] self-diffusion in polymer solutions,[25−29] colloidal suspensions,[30] and thin

*Corresponding author. E-mail: koynov@mpip-mainz.mpg.de.

 Published on Web 06/11/2009

polymer films.[31] Furthermore, it was shown that FCS can address the swelling of cross-linked polymer microbeads in organic solvents[32] and follows the process of radical polymerization of styrene over an extensive conversion range.[33]

The first FCS study of tracer diffusion in polymer melts has shown that the diffusion of a small tracer is related with the microscopic friction of the polymer matrix. However, the comparison was restricted to a single temperature, and deviations from the simple Brownian behavior were reported.[6] Here we undertake a systematic exploitation of the applicability of FCS to measure absolute values of the diffusion coefficient (D) of tracer with molecular radius, R, in polymer melts at different temperatures (T) far above their glass transition temperature (T_g). Then we discuss a possible relation between the tracer diffusion and the local segmental dynamics of the polymer host. We establish the polymer specific properties that determine $D(R,T)$ using model poly(dimethylsiloxane) (PDMS) and polyisoprene (PI) linear homopolymers with different low and high molecular weights (M_w) covering the range over which the glass transition temperatures $T_g(M_w)$ are still M_w dependent. An attempt to map the α-relaxation time $\tau(T)$ of the polymer matrix using the experimental $D(T)$ needs careful consideration since $D(T)$ corresponds to the long time diffusion with tracer mean-square displacement $\langle \Delta r^2(t) \rangle = 6Dt$ whereas at short times compared to $\tau(T)$ subdiffusive behavior is feasible. Details of the experimental methods are given in the following section. In the third section, the experimental results on tracer diffusion are discussed, and a summary of this study is given in the final section.

2. Experimental Section

2.1. Materials and Sample Preparation. Polydimethylsiloxane, PDMS (Alfa Aesar, Germany), with M_w (g/mol) ranging from 770 to 117K, 1,4-*cis*-polyisoprene, PI (PSS, Germany), with $M_w = 1.5$K, and PI (in-house synthesis) with M_w ranging from 2.5K to 33K were used as host polymers. The glass transition temperature, T_g, of all samples was measured by a differential scanning calorimeter (DSC). The molecular characteristics of the samples are listed in Table 1. A terylene dye, *N*,*N*′-bis(2,6-diisopropylphenyl)-1,6,9,14-tetraphenoxyterylene-3,4:11,12-tetracarboxidiimide (TDI), and a perylene dye, (*N*-(2,6-diisopropylphenyl)-9-(*p*-styryl)perylene-3,4-dicarboximide (PMI), were used as molecular tracers in polymer melts, as they are well dispersible in organic materials, provide high quantum yield, and show good photostability.[34−37] The chemical structures of PMI and TDI are shown along with those of the matrix polymers PI and PDMS in Scheme 1. Each tracer was first dissolved in an organic solvent, i.e., tetrahydrofuran, THF, with the concentration around 10^{-5} M, and introduced into the host polymer. Pure solvent was added to aid the mixing, and the solutions were mixed mechanically by magnetic stirrer at speed of 1000 rpm for 5−6 h. After mixing, the solvent was initially evaporated at 40 °C under vacuum for 3−4 h, and the sample was further kept under vacuum at room temperature for 1−2 weeks. To ensure that the solvent was completely evaporated, the FCS measurements were repeated after leaving the samples in vacuum for another 2 weeks. In all FCS measurements the absolute dye concentration (after solvent evaporation) was controlled in a nanomolar range.

In order to study the diffusion dynamics of small molecules in a miscible blend, poly(vinylethylene) (PVE) (PSS, Mainz, Germany), with M_w of 3.7K was mixed with 1,4-*cis*-polyisoprene (PI) with M_w of 3.5K at 0.5 weight fraction. The preparation of the blend was done by dissolving both polymers in THF and stirring the solution overnight. In this step, a terrylene dye was added. Then the solvent was evaporated under vacuum for a few weeks. The concentration of dye in the solvent free sample was controlled to be in the nanomolar range.

Scheme 1. Molecular Structures of (a) PMI, (b) TDI Dye, (c) PDMS, and (d) *cis*-1,4-PI

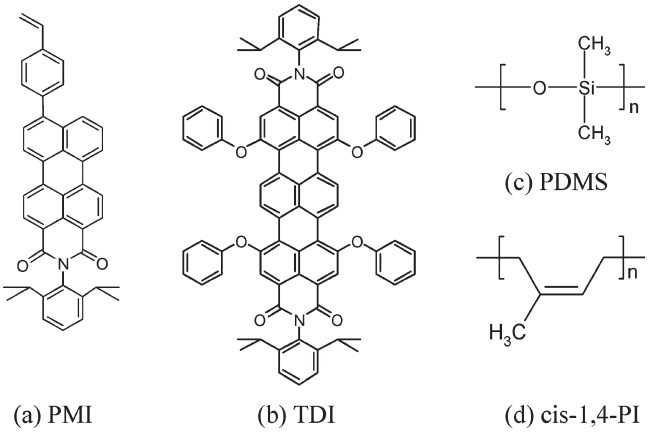

Table 1. Sources and Molecular Characteristics of the Polymer Samples

polymers	source	M_w (g/mol)	M_w/M_n	T_g (°C)
PDMS	Alfa Aesar, Germany	770	1.24	−136.0
		2000	1.40	−129.5
		4000	1.75	−127.8
		6000	1.80	−127.0
		14000	1.89	−126.1
		28000	1.75	−125.8
		63000	1.71	−125.4
		117000	1.73	−125.3
	in-house synthesis (MPIP)	5800	1.07	−127.1
		11820	1.10	−126.5
		20820	1.12	−125.7
		33880	1.05	−125.8
		59000	1.06	−125.8
		66280	1.07	−125.4
PI-1,4	PSS, Germany	1450	1.10	−81.2
	in-house synthesis (MPIP)	2580	1.21	−82.1
		3420	1.07	−71.6
		6770	1.06	−67.6
		12670	1.04	−64.3
		23000	1.06	−64.6
		33000	1.09	−64.6
PVE	PSS, Germany	3690	1.06	−22.7

2.2. Techniques. *Fluorescence Correlation Spectroscopy*. The FCS measurements were performed on a commercial setup (Carl Zeiss, Jena, Germany) consisting of the module ConfoCor 2 and an inverted microscope model Axiovert 200. A 40× Plan Neofluar objective with a numerical aperture of 0.9 and oil as immersion liquid were used in this study. The terrylene dye was excited by a HeNe laser at 633 nm, and the emission was collected after filtering with LP650 long pass filter. In the case of perylene dye, we used Ar^+ laser (488 nm) for excitation, and the emission was collected after filtering with a BP530-600 bandpass filter. For detection, an avalanche photodiode enabling single-photon counting was used. The average photon count rate was around 20−40 kHz. Since polyisoprene samples displayed intrinsic fluorescence when excited at $\lambda \sim 450-560$ nm, we used only terrylene dye with $\lambda_{ex} \sim 633$ nm as a tracer in PI. An Attofluor cell chamber (Invitrogen, Leiden, The Netherlands) with a microscope glass slide, with diameter of 25 mm and thickness of 0.15 mm, was used as a sample cell. For temperature control, a Linkam PE94 temperature control system (Linkam, Surrey, UK) was mounted on the microscope. A thermal couple wire was immersed in the sample to measure the actual temperature. During FCS measurements, the temperature was kept constant ($\Delta T < 0.5$ °C). For each sample, measurements with total duration of 10−60 min were performed. The final results were obtained as an average of 3−4 experiments performed with

different sample loading. To avoid malfunction of the objective in the present experimental setup, the studied temperature was allowed to range from 5 to 45 °C.

Dielectric Spectroscopy. Frequency- and temperature-dependent dielectric measurements were performed using an experimental setup of Novocontrol. The system was equipped with an Alpha high-resolution dielectric analyzer and temperature controller Quatro version 4.0. The samples were sandwiched between two brass disks with diameters of 20 mm, forming a flat parallel plate capacitor with thickness of 50 μm, which was maintained by Teflon strips used as spacers between the electrodes. The value of ac voltage applied to the capacitor was equal to 1 V. Temperature was controlled using a nitrogen gas cryostat, and the temperature stability of the sample was better than 0.1 K. The dielectric constant $\varepsilon^*(\omega) = \varepsilon'(\omega) - i\varepsilon''(\omega)$ measured in the frequency range from 0.01 Hz to 1 MHz was represented by the empirical Havriliak and Negami equation[38]

$$\varepsilon^*(T,P,\omega) = \varepsilon_\infty(T,P) + \frac{\Delta\varepsilon(T,P)}{[1+(i\omega\tau_{HN}(T,P))^{\alpha}]^{\gamma}} + \frac{\sigma_0(T,P)}{i\varepsilon_f\omega} \quad (1)$$

where $\varepsilon_\infty(T,P)$ is the high-frequency permittivity, $\tau_{HN}(T,P)$ is the characteristic relaxation time in this equation, $\Delta\varepsilon(T,P) = \varepsilon_0(T,P) - \varepsilon_\infty(T,P)$ is the relaxation strength of the process under investigation, α and γ (with limits $0 < \alpha$, $\alpha\gamma \leq 1$) describe respectively the symmetrical and asymmetrical broadening of the distribution of relaxation times, σ_0 is the dc conductivity, and ε_f is the permittivity of free space.

3. Results and Discussion

3.1. Tracer Diffusion Coefficient. FCS is based on detecting and analyzing the fluorescence light emitted by chromophores diffusing through a small and fixed observation volume element V, formed by a laser focused into the sample of interest. As the fluorescent molecules diffuse in and out of the observation volume they cause temporal fluctuations of the detected fluorescence intensity $\delta F(t')$. For freely diffusing fluorescence species, the autocorrelation function $G(t) - 1 = \langle \delta F(t')\delta F(t'+t)\rangle / \langle F(t')\rangle^2$ can be written[19] as

$$G(t) = 1 + \left[1 + \frac{\mathrm{Tr}}{1-\mathrm{Tr}} e^{-t/\tau_{Tr}}\right] \frac{1}{N} \frac{1}{\left[1+\frac{t}{\tau_D}\right]\sqrt{1+\frac{t}{S^2\tau_D}}} \quad (2)$$

where N is the average number of diffusing particles in the observation volume. Tr and τ_{Tr} are the fraction and the decay time of the triplet state, τ_D is the diffusion time of the species, and S is the so-called structure parameter, $S = z_0/x_0$, where z_0 and x_0 represent the axial and radial dimensions of the confocal volume, respectively. The diffusion time τ_D is defined as

$$\tau_D = {x_0}^2/4D \quad (3)$$

where D is the tracer diffusion coefficient. The experimental $G(t)$ (Figure 1) is well represented by eq 2, yielding N and τ_D. However, as the value of x_0 depends strongly on the geometrical characteristics of the optical setup and the refractive index (n_s) of the sample, a suitable calibration is required. In aqueous environments, such calibration typically relies on the straightforward measurement of the characteristic diffusion time of a dye molecule with known diffusion coefficient, i.e., Rhodamine 6G.[19] In organic solvents, however, no such simple means is available. Many dye molecules tend to aggregate in organic solvents, and in contrast to aqueous systems the dyes diffusion coefficients are rarely known. To overcome these problems, recently it was suggested that the calibration of the FCS observation volume in a given solvent can be done by independent measurements of the fluorescently labeled polymer diffusion coefficient by DLS.[26,29] Here we extend this procedure to polymer melts using for calibration a solvent with similar refractive index as the respective polymer. For the estimation of x_0 in the PDMS melt with $n_{PDMS} \approx 1.4$, we used tetrahydrofuran, THF ($n_{THF} \approx 1.4$). The diffusion coefficient of perylene-labeled polystyrene (in-housed synthesis, M_w = 340 kg/mol) in diluted THF solution was measured by DLS. Then the diffusion time τ_D of the labeled PS in the same solution was measured by FCS. Finally, the corresponding value of x_0 for THF and hence PDMS was determined from eq 3. In the case of PI ($n_{PI} = 1.5$), a similar calibration procedure was applied using toluene as a calibration solvent. In this way we have determined that for the experiments performed with Ar^+ laser (excitation at 488 nm, BP530-600 emission filter) $x_0 = 0.23$ μm in PDMS. When the HeNe laser was used (excitation at 633 nm, LP650 emission filter), we had $x_0 = 0.28$ μm in PDMS and $x_0 = 0.27$ μm in PI. In all cases the value of the structure parameter was $S \approx 10$.

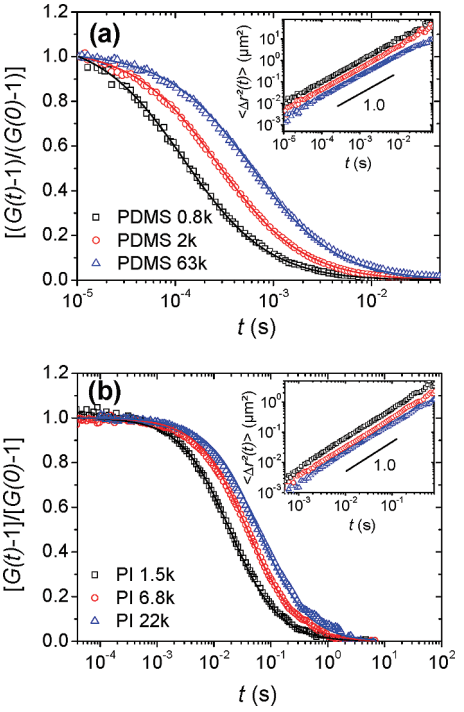

Figure 1. Normalized autocorrelation functions for the diffusion of (a) PMI in poly(dimethylsiloxane) (PDMS) and (b) TDI in polyisoprene (PI) with various molecular weights. The mean-square displacement plots in the insets conform to the slope = 1.

Figure 1 shows experimental $G(t)$ for a PMI diffusing in PDMS and TDI diffusing in PI along with the representation (solid lines) by eq 1. Owing to the ultra low fluorophore concentration, FCS allows also a computation of the tracer mean square displacement $\langle \Delta r^2(t)\rangle$ through[39]

$$G(t) = 1 + \frac{1}{N}\left(1 + \frac{2}{3}\frac{\langle \Delta r^2(t)\rangle}{{x_0}^2}\right)^{-1}\left(1 + \frac{2}{3}\frac{\langle \Delta r^2(t)\rangle}{{z_0}^2}\right)^{-1/2} \quad (4)$$

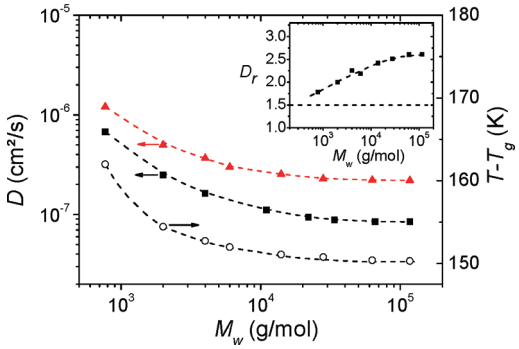

Figure 2. Diffusion coefficients of (▲) PMI and (■) TDI in polydimethylsiloxane (PDMS) matrices with different M_w at 25 °C. The variation of the distance (○) from the glass transition temperature, T_g, for the same PDMS samples is shown for comparison. Inset: the ratio, D_r, of the diffusion coefficients of perylene and terylene dye ($D_r = D_{PMI}/D_{TDI}$) in PDMS matrices. The dashed lines are to guide the eyes.

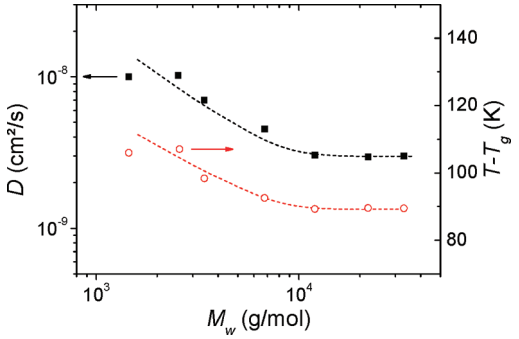

Figure 3. Diffusion coefficient of (■) TDI in polyisoprene (PI) matrices with difference M_w at 25 °C. The variation of the distance (○) from the glass transition temperature $T_g(M_w)$ for the same PI samples is shown for comparison. The dashed lines are to guide the eyes.

shown in the inset of Figure 1. For all examined polymers, these double-logarithmic plots show a slope of 1 indicative of a random Brownian diffusion of the two molecular tracers over submicrometer length scales and hence long times in the polymer matrices. We did not observed a measurable effect of the polymer polydispersity in the range $M_w/M_n < 1.8$ (Table 1) that has, therefore, a minor influence on the tracer diffusion coefficient.

The diffusion coefficient of the PMI and TDI in PDMS (eq 3) is plotted against the polymer matrix M_w in Figure 2. It decreases with M_w but reaches asymptotically a constant value above a threshold value of M_w. The molecular probe diffusion does not follow the bulk polymer viscosity, which increases strongly with M_w, above the critical M_w for entanglement, M_c ($\eta \sim M_w^{3.4}$, when $M_w > M_c \sim 30$K).[40] Instead, D becomes independent of the matrix M_w above about 30K resembling the dependence of the glass transition temperature $T_g(M_w)$ of the polymer matrix on its molecular weight; $T_g(M_w)$ (K) = 147.6(1−55.3/M_w), which is a rather weak M_w dependence. As seen in Figure 2, the variation of the quantities $T-T_g(M_w)$ (T = 298 K) and D with M_w looks alike and both quantities become asymptotically independent of M_w. It is known that the former controls the segmental mobility of bulk polymers, whereas for $D(T)$ molecular weight can have additional effects (see Figure 4). Further, it has been shown by FRAP and fluorescence nonradiative energy transfer experiments that probe size (R) may modify the scaling $D \sim R^{-1}$ in polymer melts,[3,4,7] thus rendering the dependence $D(R,T,M_w)$ very interesting.

We have compared the values of D for PMI and TDI in the PDMS matrices of Figure 2. The chemical structures shown in Scheme 1 indicate that TDI are significantly bigger than PMI. This size disparity is reflected in the hydrodynamic radii, $R_{PMI} = 0.53$ nm and $R_{TDI} = 0.8$ nm, as measured by FCS in toluene solutions. Clearly, the smaller probe (PMI) diffuses significantly faster than the bigger one (TDI) in all polymer matrices. The ratio of the diffusion coefficients of the two probes, $D_r = D_{PMI}/D_{TDI}$ plotted vs matrix molecular weight in the inset of Figure 2 increases with M_w reaching a constant value (~2.6) at sufficiently high M_w, for which T_g reaches its limiting high M_w value ($T_{g,\infty} \cong 148$ K). As expected for small tracers diffusing in polymer melts and in agreement with a recent XPCS study,[41] these values of D_r differ significantly from the predictions of the DSE equation, according to which the diffusion coefficient of small molecules is reversely proportional to their hydrodynamic radii ($D \sim (\eta R)^{-1}$), and therefore the ratio of the diffusion coefficients of the two dyes, $D_r = D_{PMI}/D_{TDI}$, should amount to about 1.5 (dashed line in the inset to Figure 2).

In a different approach[42] of a length-dependent effective viscosity $\eta'(R)$ ($< \eta$), the scaling relationship $\eta' \sim (R/b)^2$ was proposed on the ground of Rouse dynamics and Gaussian coil statistics, when the particle size R is less than the polymer coil radius (but still bigger than the persistence length), i.e., $\eta'(R) \sim N'$ where $N' \cong R^2/b^2$ is the number of monomers of a chain portion of size R. Hence, the D/D_{DSE} ratio should scale as R^{-2}. Our data, although based on only two tracers, seems to be in agreement with the latter approach.

In order to examine whether the observed characteristics of molecular tracer diffusion in PDMS are general for amorphous bulk polymers above T_g, we have also measured the TDI diffusion coefficient in PI with different M_w. The dye diffusion data plotted in Figure 3 reveal similar behavior shown for the tracer diffusion in PDMS (Figure 2); i.e., D closely follows the molecular weight dependence of the polymer glass transition temperature; $T_g(M_w)$ (K) = 209.5-(1 − 122/M_w), which is clearly stronger than for $T_g(M_w)$ of PDMS. For the consistency of these results, it is interesting to note that the PI sample with the lowest molecular weight (1.5K) has a slightly higher T_g than the PI sample with the somewhat higher M_w (2.5K) probably due to higher polydispersity of the latter (Table 1). This trend is consistently reflected in the plot of D vs M_w. An inspection of Figures 2 and 3 shows that at temperatures well above T_g the tracer diffusion is about 30 times slower in PI than in PDMS.

We consider next the effect of temperature on the tracer diffusion in polymer melts. For amorphous polymers, the temperature dependence of dynamic quantities such as viscosity, self-diffusion, or segmental α-relaxation is typically described by the non-Arrhenius eq 5. As shown in Figure 4a, the temperature dependence of D for the two dyes in PDMS (0.77K and 65K) and TDI in PI (1.5K, 3.5K, and 22K) in the range 280−320 K far above T_g can be well represented by the well-known VFT equation

$$D = D_\infty \exp\left[-\frac{B_D}{R^*(T-T_0)}\right] \quad (5)$$

where D_∞ is the limiting high-temperature value of D, $T_0 = T_g - c_2$ is the ideal glass transition temperature, R^* is the gas constant, and the value of the constant c_2 was assumed to be 20 and 50 K for PDMS[43] and PI,[44] respectively. The temperature dependence of PMI diffusion in both polymeric matrices is well represented by eq 5 (dashed lines in Figure 4a) using only D_∞ and B_D as adjustable parameters. The values of the activation parameters are listed in Table 2

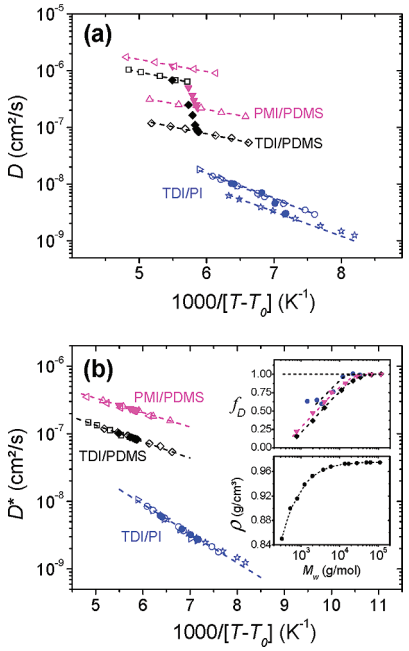

Figure 4. (a) Temperature dependence of the diffusion coefficient, D, of PMI in (left-pointing △) PDMS-0.8 and (△) PDMS-65 and TDI in (□) PDMS-0.8, (◇) PDMS-65, (right-pointing △) PI-1.5, (○) PI-3.5, and (☆) PI-22 where $T_0(M_w) = T_g(M_w) - c_2$; $c_2 = 20$ and 50 K for PDMS and PI, respectively. This plot includes D of PMI (▼) and TDI in (◆) PDMS and TDI in (●) PI melts from the room temperature measurements of 2Figures 2 and 3. Dashed lines denote the representation of the data by eq 5. (b) Superimposed tracer diffusion coefficients $D^* = f_D D(T)$ vs $T - T_0(M_w)$ with the shifting factor $f_D(M_w)$ for PMI in (▼) PDMS, TDI in (◆) PDMS, and TDI in (○) PI) given in the upper inset. Lower inset shows the molecular weight dependence of PDMS density, $\rho(M_w)$.

along with the fixed values of T_0. These characteristic parameters reveal some pertinent polymer and tracer specific differences:

(a) The value of B_D is virtually independent of the matrix M_w as indicated by the parallel temperature dependence of D in the two systems and this insensitivity of D to M_w variation applies for both dyes (in PDMS). Since B_D is related to the activation energy necessary to create a hole with size equal to the minimum size for displacement of the penetrant molecule,[45] its value is expectedly found to be M_w independent.

(b) The activation energy B_D does depend, however, on the tracer size; $B_D(R)$ amounts to 4.1 ± 0.1 and 4.7 ± 0.2 kJ/mol respectively for the small (PMI) and larger (TDI) dye in PDMS. If we envisage both tracers as rigid objects, then the necessary free volume hole to enable diffusion is proportional to the tracer size and hence the associated activation energy should be higher for the larger tracer.

(c) Diffusion coefficient of TDI in PDMS is much bigger (about 30 times, see Figures 2 and 3) than in PI at temperatures equidistant from T_g. The differences in the value of D_∞ (Table 2) cannot rationalize this disparity. Alternatively, the effect is related to the activation energy, which value for TDI in PI $B_D = 8.3 \pm 0.5$ kJ/mol (Table 2) is almost twice bigger than in PDMS. Notably B_D for PDMS is one of the lowest values reported for polymers in the literature.[46]

(d) The data shown in Figure 4a imply that there is an additional M_w dependence on $D(M_w)$ which is not attributed to $T_g(M_w)$. Owning to the molecular weight dependence of T_g, the isothermal tracer diffusion data of Figures 2 and 3 respectively for PDMS (solid down triangles for PMI and solid diamond for TDI) and PI (solid circles for TDI) in Figure 4a bridge nicely the gap between the two extreme M_w matrices. Hence, the extra M_w dependence is attributed to the limiting high temperature tracer diffusion D_∞ in eq 5.

Table 2. Activation Parameters (Eq 5)

tracer	polymer	D_∞ (10^{-6} cm^2/s)	B_D (kJ/mol)	T_0 (K)[a]
PMI	PDMS-0.8	18.3 ± 0.07	4.1 ± 0.1	116
	PDMS-65	3.9 ± 0.02	4.1 ± 0.1	128
TDI	PDMS-0.8	15.6 ± 0.12	4.7 ± 0.2	116
	PDMS-65	2.2 ± 0.02	4.7 ± 0.2	128
TDI	PI-1.5	6.3 ± 0.15	8.3 ± 0.5	142
	PI-3.5	5.9 ± 0.04	8.3 ± 0.5	152
	PI-22	3.6 ± 0.06	8.3 ± 0.5	159

[a] $T_0 = T_g - c_2$, $c_2 = 20$ K for PDMS and 50 K for PI.

This finding, along with the M_w-independent B_D (see (a) above) allows a normalization of the data of Figure 4a by a vertical shifting factor $f_D = D_\infty(\text{high } M_w)/D_\infty(M_w)$ where $D_\infty(\text{high } M_w)$ denotes the asymptotic value of D_∞ for the highest M_w in Figure 4a. This successful superposition is shown in Figure 4b, whereas the corresponding values of f_D are plotted in the upper inset of the same figure underlying the characteristic $D_\infty(M_w)$ for the two systems. This additional molecular weight dependence can be attributed to the variation of density ρ with M_w, as indicated by the qualitative agreement between $\rho(M_w)$ and $D_\infty(M_w)$ in PDMS visualized in the two insets to Figure 4b. Apparently, the dependence of D on the polymer density can not be solely accounted for by the variation of T_g with density.

Summing up this section, eq 5 describes well the dependence of the tracer diffusion coefficient $D(R,M_w,T)$ on temperature, matrix M_w, and tracer size with a M_w-dependent prefactor, $D_\infty(M_w)$, a size-dependent activation parameter, $B_D(R)$, and the anticipated M_w-dependent glass transition $T_g(M_w)$.

3.2. Does the Tracer Diffusion Relate to the Polymer Host Segmental Dynamics? Figure 5 is a compilation of the segmental relaxation times, τ (solid squares),[47] and the tracer diffusion coefficients (open squares) in PI-1.5K at different temperatures. The former have been obtained from dielectric spectroscopy (DS) experiments and are in good agreement with molecular dynamics simulations. The data are shown in an Arrhenius representation as in the original work.[47] Interestingly, the $D(T)$ data, which were well fitted with VFT equation (eq 5) as discussed above, are represented reasonably well also by an Arrhenius type of plot. This is most likely related to the relatively limited temperature range of our experiments (5−45 °C) and the fact that all measurements were performed at temperatures well above the glass transition of the polymers. The comparison shown in the main Figure 5 indicates that over overlapping temperature range the tracer diffusion coefficient D in the PI matrix and its segmental relaxation time exhibit similar temperature dependences. In the following we try to relate the measured tracer diffusion coefficient D with the segmental dynamics of the polymer matrix.

As discussed in section 3.1, the long time diffusion of a molecular penetrant is an a priori unknown function of its size and matrix M_w and depends on temperature according to eq 5. For the extremely low tracer concentrations of the diffusant used in this study, the ideal temperature $T_0(M_w)$ is undoubtedly a property of the host polymer matrix only, whereas this cannot be generally assumed for the activation parameter B_D. In the absence of specific penetrant−polymer interactions, the two tracers (PMI, TDI) exhibit an activation energy which is independent of PDMS M_w but depends on the penetrant size.

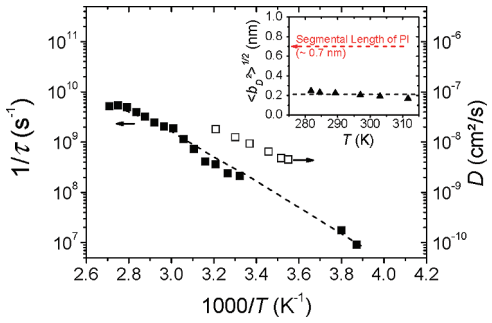

Figure 5. Temperature dependence of the segmental relaxation time τ (■) of the bulk PI-1.5K[47] and the tracer diffusion D (□) of TDI in the same PI matrix at temperatures far above T_g. The characteristic length (▲) $\langle b_D^2\rangle^{1/2}$ ($\langle b_D^2\rangle = 6D\tau$) is shown in the inset.

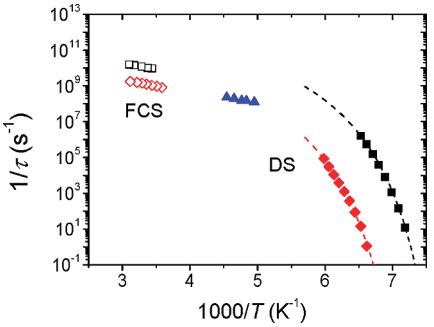

Figure 6. Temperature dependence of the segmental relaxation time τ of PDMS with M_w of 0.77K (■) and 65K (◆) as measured by DS at low temperatures and (open symbols) estimated by FCS at high temperatures. Literature data for PDMS with M_w of 1.4K (▲) obtained by dielectric spectroscopy at intermediate temperatures[44] are also shown for comparison. Dashed lines denote the representation of the DS segmental relaxation frequencies by VFT equation.

The tracer specific $B_D(R)$ implies that the temperature dependent factor in eq 5 is not determined solely by the polymer matrix. For a given tracer however the Einstein diffusion relation, $\langle b^2\rangle = 6D\tau$, can be used[6,7] to define an arbitrary average displacement length $\langle b^2\rangle^{1/2}$ for the time of one segmental relaxation. Such a definition has been already used in the literature[6,7] and is based on the (strong) assumption that the short time diffusion of the tracer, D_s, is the same as the long time diffusion coefficient, D. Furthermore, this $\langle b^2\rangle^{1/2}$ can be considered temperature independent only if the activation energy for the tracer diffusion, $B_D(R)$, is equal to the activation parameter for the polymer segmental relaxation, B.

Next we attempt a critical assessment of the two assumptions, i.e., (i) $B_D(R) \cong B$ and (ii) $D_s \cong D$, through a direct comparison of the experimental D and τ for the PI sample of Figure 5. The reported[48] value of B for PI measured at temperatures near T_g is 1035 K (8.6 kJ/mol), very close to the value of B_D at temperatures far above T_g but smaller than the value of B (~1570 ± 60 K or 13 ± 0.5 kJ/mol) evaluated from the segmental times[47] at temperatures far above T_g; the latter measurements are more difficult and subject to a large error. Hence, the more precise D data at high temperatures become very relevant and appear to relax assumption (i) in the computation of $\langle b_D^2\rangle^{1/2}$. Noteworthy, the "average displacement length" $\langle b_D^2\rangle^{1/2}$ was reported[7] to depend strongly on the type of the tracer and more importantly on the distance $T - T_g$ reflecting the enhancement of dynamics heterogeneity in the polymer host.

Concerning the second assumption, $D_s \cong D$ (see also the Appendix), it should be stressed that FCS measures the tracer diffusion coefficient D over a length scale of few hundred nanometers, i.e., orders of magnitude larger than the polymer segment dimension (Kuhn segment), b (inset to Figure 5). It is well-known from molecular dynamics simulations studies of polymer/tracer systems at temperatures far above T_g[14−18,49,50] that at shorter time scale the relation between mean-squared displacement and time is strongly nonlinear. In this respect the computation of $\langle b_D^2\rangle^{1/2}$ from FCS data is somewhat ambiguous and should not be considered as a direct measure for the tracer displacement on the extremely short time scale of the segmental relaxation.

Furthermore, a generalization of the molecular dynamics simulations for a different polymer/penetrant system (PS/EB, see Appendix) to the case of PI shows that the real displacement of the tracer during the segmental relaxation time is much larger than $\langle b_D^2\rangle^{1/2}$; in the initial subdiffusive regime the effective tracer diffusion exceeds D. In the absence of a molecular theory, computer simulations can provide the necessary system specific information.

In spite of the above discussion, and since data about the initial subdiffusive regime are rarely available, the rationalization of the $\langle b_D^2\rangle^{1/2}$ value for PI allows to estimate values of τ for other flexible melts far above T_g. Here, we utilized this semiempirical approach to estimate the missing values of τ for PDMS at temperatures well above T_g from the TDI diffusion data (Figure 4); dielectric spectroscopy (DS) yields the segmental relaxation times[44,51] of PDMS only near T_g. For a direct comparison with the present FCS results, we have measured τ of PDMS with M_w of 770 and 65 K near T_g using DS.

Figure 6 shows these values of τ along with the estimated τ ($= \langle b_D^2\rangle/6D$) at high temperatures. Apparently, a single VFT cannot represent both sets and moreover the predicted relaxation frequency ($1/\tau$) for the two PDMS melts at high temperatures are slower than the extrapolated DS relaxation frequencies. While this discrepancy may originate from the limitations of the used semiempirical approach, it can be also attributed to different segmental dynamics of PDMS at low and high temperatures. In fact, this is a proposition made earlier based on the deviation from a single VFT at intermediate temperatures,[44] as indicated in Figure 6.

The proposed relation between long time tracer diffusion and segmental relaxation times of the polymer matrix is not fundamental as discussed in this section and will be further addressed below. Nevertheless small molecule tracer diffusion can yield an information on the segmental relaxation and its temperature dependence after calibration of the average microscopic displacement length, $\langle b_D^2\rangle^{1/2}$.

3.3. Tracer Diffusion in a Miscible Polymer Blend. It is known that miscible polymer blends exhibit two distinct segmental relaxation times due to local composition inhomogeneities inherent to the nanoscopic cooperative length associated with the primary α-relaxation. Over larger length scales the system is spatially homogeneous displaying a single composition averaged glass transition temperature. In fact, pulsed-field gradient NMR reveals a single average friction in agreement with viscosity and T_g measurements.[52] We have selected the well studied 1,4-*cis*-polyisoprene (PI M_w ~ 3.5K, T_g = 201 K) and poly(vinylethylene) (PVE, M_w ~ 3.7K, T_g = 250 K) miscible blend,[49] in order to explore its composition homogeneity by FCS tracer diffusion experiments. Figure 7 shows that the experimental normalized $G(t)$ for the TDI diffusion in the symmetric PI/PVE blend is well described by a single Fickian diffusion process (eq 2) as also seen in the inset. The diffusivity in the blend is intermediate

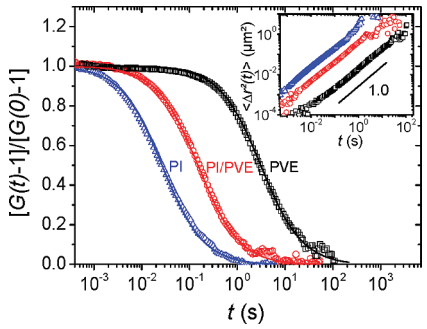

Figure 7. Normalized fluorescence intensity autocorrelation function for the TDI diffusion in 1,4-*cis*-polyisoprene 3.5K (PI) (△), poly (vinylethylene) 3.7K (PVE) (□), and their symmetric (50 wt %) blend (○). The solid lines denote one component fits of eq 2. The mean-square displacement plots in the insets indicate Fickian diffusion behavior.

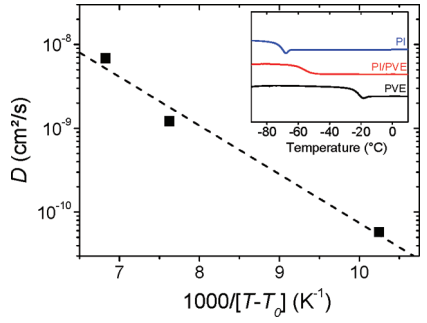

Figure 8. Tracer diffusion coefficient of TDI in PI, PVE, and the symmetric (50 wt %) PI/PVE blend at 298 K plotted as a function of the distance from the ideal temperature T_0. Dashed line is fitted with the parameters shown in text. Inset: DSC traces for the three systems.

between its constituents being closer to the tracer diffusion in PI at the same temperature.

This comparison is quantified in the VFT (eq 5) plot of Figure 8 which shows the tracer diffusion coefficient D vs $1/[T - T_0]$, where $T_0 = T_g - 50$ K and T_g is the glass transition temperature in the blend and its constituent components obtained by the DSC traces (inset to Figure 8). Equation 5 represents well (dashed line in Figure 8) the experimental D using $D_\infty = 5 \times 10^{-5}$ cm^2/s and $B_D = 11.2$ kJ/mol.

The diffusion coefficient in the blend is closer to the faster component, PI, resembling the relation between the T_g values. The DSC trace is broader in the blend reflecting composition fluctuations.

Conversely, the diffusion of the molecular tracer over few hundreds nanometers senses an effective medium with a single composition average T_g conforming to the Fox−Flory linear composition relation of the reciprocal T_g.

4. Conclusions

We used fluorescence correlation spectroscopy to measure the diffusion coefficient of small molecule chromophores in bulk PDMS, PI, and PVE homopolymers with different molecular weights (M_w) at temperatures well above the polymer glass transition, T_g. The unique, single molecule sensitivity of the FCS technique allows studies at nanomolar tracer concentrations, ensuring that the penetrants do not modify the matrix polymer properties. For all systems we observed that the diffusion rate does not follow the surrounding viscosity, which is extremely increased for high-M_w polymers. Instead, the diffusion coefficient D of small tracer is strongly correlated to the polymer segmental dynamics while it keeps particle characteristics. We found that the activation barrier $B_D(R)$ in the temperature dependence of $D(T,M_w,R)$ (eq 5) increases with the tracer size R and is insensitive to the variation of matrix M_w.

For a molecular tracer (TDI), we found that the temperature dependence of D in low molecular weight PI is similar to that of the segmental relaxation time τ, as measured by dielectric spectroscopy and depolarized Rayleigh scattering. Comparing these two processes, the average displacement $\langle b^2\rangle^{1/2} = (6D\tau)^{1/2}$ of the tracer during the period for reorientation of the polymer segment was evaluated. We found $\langle b^2\rangle^{1/2} \approx 0.2$ nm in the studied temperature range of 5−45 °C. This value is relatively small because of two reasons: (i) The TDI molecule is still large, compared to the monomer of PI and PDMS; we anticipate that with growing size of the additive $\langle b^2\rangle^{1/2} \to 0$. (ii) There is no information about the short time dynamics (see eq A-1 in the Appendix) since D represents the long time tracer diffusion (over a length scale few hundred nanometers) Nevertheless, using this value of $\langle b^2\rangle^{1/2}$, we applied FCS to estimate in a semiempirical approach the segmental relaxation time τ of several PDMS samples with different molecular weights at temperatures well above their T_g.

The global nature of the molecular tracer diffusion coefficient D in the FCS experiment was examined in the case of the miscible polymer blend PI/PVE . While such blend exhibits two distinct α-relaxations we observed a single diffusion coefficient D for a TDI probe. The effect is caused by the long length scale of the FCS experiments (∼500 nm) that average the two α-relaxations contributions. Furthermore, the value of the diffusion coefficient in the blend is closer to the faster component, PI, resembling the relation between the T_g values.

Acknowledgment. We thank Hans-Jürgen Butt for the helpful discussions, Klaus Müllen and Kalina Peneva for synthesis of perylene and terrylene dyes, and A. Best, A. Hanewald, T. Wagner, J. Thiel, and Polymer Analytic service group at MPIP for the technical assistance. T. C. thanks Marie Curie fellowship for early stage research training (EST) for the financial support. P.V. thanks GSST (PENED-2003/856) and EU-NANODIRECT CP FP213948-2 for financial support.

Appendix

Molecular Probe Diffusion and Segmental Dynamics in Polymer Melts through Molecular Dynamics Simulations. As it was discussed in the Introduction, any experimental or simulation work that can yield information about the dynamics of a tracer in a polymer matrix is of particular importance. An empirical connection between the mobility of a specific penetrant (at fixed temperature) and the dynamics of the polymer matrix has been proposed by defining the average distance the penetrant moves for times equal to the segmental relaxation time of the matrix, $\langle b^2\rangle^{1/2}$ (see also section 3.2). Such an "average displacement length" has been used in the past in the analysis of experimental data, and it is defined as $\langle b^2\rangle^{1/2} = (6D\tau)^{1/2}$ with D being the *long-time* diffusion of the penetrant and τ the segmental relaxation time of the polymer matrix.[6,7]

In general, the above relation is not accurate since it is based on the assumption that *long time* diffusion coefficient of the penetrant is related in a very simple way to the segmental dynamics of the matrix, which usually occurs at much shorter time scales. On the contrary, it is well known that the dynamics of polymers as well as polymer/penetrant mixtures is non-Fickian in short time regimes, i.e., the mean-square displacement, ΔR ($\Delta R \equiv (\mathbf{R}(t) - \mathbf{R}(0)^2)$, of a molecule evolves with time as $\langle \Delta R\rangle \sim t^\alpha$ with $\alpha < 1$. For example, in the small time regime (times shorter than the longest relaxation time) chain center-of-mass of polymers exhibits well known non-Fickian subdiffusive behavior,[53−55] related with

the correlation hole cage, where $\alpha = 0.8$. The corresponding slope for the mean-square displacement of segments is about 0.5 for unentangled systems (Rouse model), whereas for entangled systems it is more complicated exhibiting four different power law regimes (reptation theory).[54] For the case of penetrant/polymer mixtures, the situation is even more complicated since the subdiffusive behavior of the penetrant is a result of the coupling between the tracer molecule and the polymer matrix. A more accurate estimation of an "average displacement length", including information about the mobility of penetrant at all times, can be given through

$$\langle b^2 \rangle^{1/2} = \left(\int_0^\tau 6D(t)\, dt \right)^{1/2} \qquad \text{(A-1)}$$

where the time-dependent (effective) diffusion coefficient of the penetrant is defined as $D(t) = \langle (\mathbf{R}_{tr}(t) - \mathbf{R}_{tr}(0)^2 \rangle / 6t$ with $\mathbf{R}_{tr}(t)$ and $\mathbf{R}_{tr}(0)$ being the position of the tracer molecule at time t and 0, respectively, and the brackets denote the statistical average.

It is clear that in order to use eq A-1 detailed information about the mobility of the penetrant in the short time subdiffusive regime is needed. A direct way to obtain such information is to use, if possible, detailed atomistic MD simulations and accurately calculate the integral in eq A-1. Then a detailed study combining the simulation results and the experimental data it would have been possible. However, this requires experimental measurements and detailed atomistic simulations for exactly the same systems, and it is beyond the scope of this work. What we present here is a detailed analysis, along the lines of the above discussion, of a polymer/penetrant system (polystyrene/ethylbenzene, PS/EB) studied recently through MD simulations and NMR experiments.[50] In more detail united atom (UA) MD simulations of various PS/EB systems have been performed, and the diffusion of EB has been calculated for various concentrations of EB and temperatures. In Figure 9 we present the effective diffusivity of EB in a PS matrix ($M_w = 10\,000$ g/mol) for a PS/EB system with very low concentration of EB ($w_{EB} = 0.01$) at $T = 463$ K. As we can see, the effective diffusion coefficient of EB is higher at short times (subdiffusive regime), whereas at longer times (Fickian regime) reaches a time-independent value, which correspond to the diffusion coefficient reported. Note that error bars in the atomistic data are essentially zero in the short time regime, whereas in the long time regime they are much larger (shown with symbol). Apparently, the neglect of the short time dynamics is expected to give a smaller value for $\langle b^2 \rangle^{1/2}$ than the real one.

In order to proceed and calculate $\langle b^2 \rangle^{1/2}$ through eq A-1, we also need an estimation of the segmental relaxation time of the polymer matrix, τ. A common way to study segmental relaxation is by calculating a time correlation function of a vector, v_b, representing a chemical bond or a bond vector within a monomer. The reorientation of such a vector can be studied by considering ensemble-averaged of the second Legendre polynomial, $P_2(t)$ ($P_2(t) = {}^3/_2\langle \cos^2(\theta) \rangle - {}^1/_2$), where θ is the angle of v_b bond at time t relative to its original position and the segmental correlation time τ is defined as the integral of $P_2(t)/P_2(0)$. In the case of PS/EB systems, $\tau = 2.8 \pm 0.5$ ns at 463 K using for v_b the CH−CH$_2$ backbone bond in the united atom representation. And from eq A-1, we obtain $\langle b^2 \rangle^{1/2} = 2.4 \pm 0.1$ nm. Alternatively, if we know τ, $\langle b^2 \rangle^{1/2}$ can be directly calculated from the mean-square displacement of the simulation trajectory; this gives of course exactly the same result. This value is, as expected, larger than the one predicted by using the long-time diffusion of the penetrant (in that case $\langle b^2 \rangle^{1/2} = 2.2 \pm 0.1$ nm). This difference would be even higher for tracers larger than EB, like those studied here experimentally (TDI and PMI). The value of $\langle b^2 \rangle^{1/2}$ predicted here is about the order of the Kuhn length of the polymer matrix, b_K ($b_K \cong 1.5$ nm). We should also note that the UA MD simulations performed here predict about an order of magnitude faster diffusion of EB molecules in the PS/EB systems, comparing to the real one obtained from NMR measurements.[50] However, at the same time the segmental dynamics of the UA polymer is also about the same order faster than the real one (i.e., the segmental relaxation time is shorter).[55] Therefore, we expect that the value predicted here for $\langle b^2 \rangle^{1/2}$ is very close to the real one. Finally, as it was presented elsewhere,[50] the intermolecular monomer structure between EB and PS molecules shows a structure for distances up to about 2 nm. This means that the EB molecules move in a local cage of about 2 nm, and one would expect that for such distances the penetrant would exhibit non-Fickian diffusion.

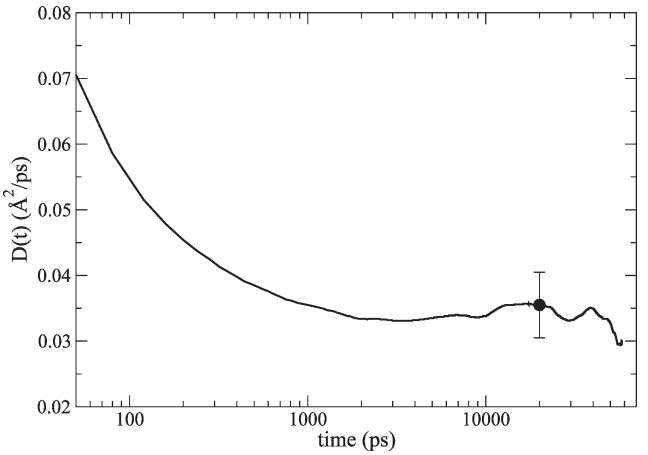

Figure 9. Time-dependent diffusion coefficient of EB in PS matrix obtained from UA MD simulations ($w_{EB} = 0.01$, $T = 463$ K).

References and Notes

(1) Ehlich, D.; Sillescu, H. *Macromolecules* **1990**, *23* (6), 1600–1610.
(2) Cicerone, M. T.; Blackburn, F. R.; Ediger, M. D. *Macromolecules* **1995**, *28* (24), 8224–8232.
(3) Deppe, D. D.; Miller, R. D.; Torkelson, J. M. *J. Polym. Sci., Part B: Polym. Phys.* **1996**, *34*, 2987–2997.
(4) Hall, D. B.; Deppe, D. D.; Hamilton, K. E.; Dhinojwala, A.; Torkelson, J. M. *J. Non-Cryst. Solids* **1998**, *235−237* (235), 48–56.
(5) Ediger, M. D. *Annu. Rev. Phys. Chem.* **2000**, *51*, 99–128.
(6) Best, A.; Pakula, T.; Fytas, G. *Macromolecules* **2005**, *38* (10), 4539–4541.
(7) Maji, S.; Urakawa, O.; Adachi, K. *Polymer* **2007**, *48*, 1343–1351.
(8) Rajian, J. R.; Quitevis, E. L. *J. Chem. Phys.* **2007**, *126* (224506), 224506-1−10.
(9) Bueche, F. *Physical Properties of Polymers*; Interscience: New York, 1962.
(10) Vrentas, J. S.; Duda, J. L. *J. Appl. Polym. Sci.* **1978**, *22* (8), 2325–2339.
(11) Vrentas, J. S.; Vrentas, C. M. *Macromolecules* **1993**, *26* (6), 1277–1281.
(12) von Meerwall, E.; Feick, E. J.; Ozisik, R.; Mattice, W. L. *J. Chem. Phys.* **1999**, *111* (2), 750–757.
(13) Adachi, K. *Macromolecules* **1990**, *23* (6), 1816–1821.
(14) Harmandaris, V. A.; Angelopoulou, D.; Mavrantzas, V. G.; Theodorou, D. N. *J. Chem. Phys.* **2002**, *116* (17), 7656–7665.
(15) Muller-Plathe, F.; Rogers, S. C.; Vangunsteren, W. F. *Chem. Phys. Lett.* **1992**, *199* (3−4), 237–243.
(16) Gusev, A. A.; Suter, U. W. *J. Chem. Phys.* **1993**, *99* (3), 2228–2234.

(17) Theodorou, D. N. Molecular Simulations of Sorption and Diffusion in Amorphous Polymers. In *Diffusion in Polymers*; Neogi, P., Ed.; Marcel Dekker: New York, 1996.
(18) Hahn, O.; Mooney, D. A.; Muller-Plathe, F.; Kremer, K. *J. Chem. Phys.* **1999**, *111* (13), 6061–6068.
(19) Rigler, R.; Elson, E. *Fluorescence Correlation Spectroscopy*; Springer-Verlag: New York, 2001.
(20) Kim, B. S.; Lebedeva, O. V.; Koynov, K.; Gong, H.; Glasser, G.; Lieberwith, I.; Vinogradova, O. I. *Macromolecules* **2005**, *38* (12), 5214–5222.
(21) Koynov, K.; Mihov, G.; Mondeshki, M.; Moon, C.; Spiess, H. W.; Mullen, K.; Butt, H.-J.; Floudas, G. *Biomacromolecules* **2007**, *8* (5), 1745–1750.
(22) Sukhishvili, S. A.; Chen, Y.; Muller, J. D.; Gratton, E.; Schweizer, K. S.; Granick, S. *Macromolecules* **2002**, *35* (5), 1776–1784.
(23) Zhao, J.; Granick, S. *Macromolecules* **2007**, *40* (4), 1243–1247.
(24) Gianneli, M.; Beines, P. W.; Roskamp, R. F.; Koynov, K.; Fytas, G.; Knoll, W. *J. Phys. Chem. C* **2007**, *111* (35), 13205–13211.
(25) Zettl, H.; Hafner, W.; Boker, A.; Schmalz, H.; Lanzendorfer, M.; Muller, A. H. E.; Krausch, G. *Macromolecules* **2004**, *37* (5), 1917–1920.
(26) Liu, R.; Gao, X.; Adams, J.; Oppermann, W. *Macromolecules* **2005**, *38* (21), 8845–8849.
(27) Zettl, H.; Zettl, U.; Krausch, G. *Phys. Rev. E* **2007**, *75*, 061804.
(28) Grabowski, C. A.; Mukhopadhyay, A. *Macromolecules* **2008**, *41* (16), 6191–6194.
(29) Cherdhirankorn, T.; Best, A.; Koynov, K.; Peneva, K.; Muellen, K.; Fytas, G. *J. Phys. Chem. B* **2009**, *113* (11), 3355–3359.
(30) Kang, K.; Gapinski, J.; Lettinga, M. P.; Buitenhuis, J.; Meier, G.; Ratajczyk, M.; Dhont, J. K. G.; Patkowski, A. *J. Chem. Phys.* **2005**, *122*, 044905.
(31) Casoli, A.; Schonhoff, M. *Biol. Chem.* **2001**, *382*, 363–369.
(32) Zhang, R.; Cherdhirankorn, T.; Graf, K.; Koynov, K.; Berger, R. *Microelectron. Eng.* **2008**, *85*, 1261–1264.
(33) Woell, D.; Uji-i, H.; Schnitzler, T.; Hotta, J. I.; Dedecker, P.; Herrmann, A.; De Schryver, F. C.; Muellen, K.; Hofkens, J. *Angew. Chem., Int. Ed.* **2008**, *47* (4), 783–787.
(34) Herrmann, A.; Müllen, K. *Chem. Lett.* **2006**, *35* (9), 978–985.
(35) Jung, C.; Müller, B. K.; Lamb, D. C.; Nolde, F.; Müllen, K.; Bräuchle, C. *J. Am. Chem. Soc.* **2006**, *128* (15), 5283–5291.
(36) Nolde, F.; Qu, J. Q.; Kohl, C.; Pschirer, N. G.; Reuther, E.; Müllen, K. *Chem.—Eur. J.* **2005**, *11* (13), 3959–3967.
(37) Uji-i, H.; Melnikov, S. M.; Deres, A.; Bergamini, G.; de Schryver, F.; Herrmann, A.; Mullen, K.; Enderlein, J.; Hofkens, J. *Polymer* **2006**, *47* (7), 2511–2518.
(38) Havriliak, S.; Negami, S. *Polymer* **1967**, *8*, 161.
(39) Shusterman, R.; Alon, S.; Gavrinyov, T.; Krichevsky, O. *Phys. Rev. Lett.* **2004**, *92* (4), 048303-1–4.
(40) Berry, G. C.; Fox, T. G. *Advances in Polymer Science*; Springer: Berlin, 1968; Vol. 5, pp 261−357.
(41) Tuteja, A.; Mackay, M. E.; Narayanan, S.; Asokan, S.; Wong, M. S. *Nano Lett.* **2007**, *7* (5), 1276–1281.
(42) Brochard Wyart, F.; de Gennes, P. G. *Eur. Phys. J. E* **2000**, *1*, 93–97.
(43) Kirst, K. U.; Kremer, F.; Pakula, T.; Hollingshurst, J. *Colloid Polym. Sci.* **1994**, *272* (11), 1420–1429.
(44) Kremer, F.; Schönhals, A. *Broadband Dielectric Spectroscopy*; Springer-Verlag: Berlin, 2003.
(45) Ferry, J. D. *Viscoelastic Properties of Polymers*; John Wiley and Sons: New York, 1980.
(46) Chen, S. P.; Ferry, J. D. *Macromolecules* **1968**, *1* (3), 270–278.
(47) Doxastakis, M.; Theodorou, D. N.; Fytas, G.; Kremer, F.; Faller, R.; Müller-Plathe, F.; Hadjichristidis, N. *J. Chem. Phys.* **2003**, *119* (13), 6883–6894.
(48) Boese, D.; Kremer, F. *Macromolecules* **1990**, *23* (3), 829–835.
(49) Doxastakis, M.; Kitsiou, M.; Fytas, G.; Theodorou, D. N.; Hadjichristidis, N.; Meier, G.; Frick, B. *J. Chem. Phys.* **2000**, *112* (19), 8687–8694.
(50) Harmandaris, V. A.; Adhikari, N. P.; van der Vegt, N. F. A.; Kremer, K.; Mann, B. A.; Voelkel, R.; Weiss, H.; Liew, C. C. *Macromolecules* **2007**, *40* (19), 7026–7035.
(51) Lund, R.; Alegria, A.; Goitandia, L.; Colmenero, J.; Gonzalez, M. A.; Lindner, P. *Macromolecules* **2008**, *41* (4), 1364–1376.
(52) Doxastakis, M.; Chrissopoulou, K.; Aouadi, A.; Frick, B.; Lodge, T. P.; Fytas, G. *J. Chem. Phys.* **2002**, *116* (11), 4707–4714.
(53) Paul, W.; Binder, K.; Kremer, K.; Heermann, D. W. *Macromolecules* **1991**, *24* (23), 6332–6334.
(54) Doi, M.; Edwards, S. F. *The Theory of Polymer Dynamics*; Clarendon Press: Oxford, 1986.
(55) Harmandaris, V. A.; Kremer, K. *Macromolecules* **2009**, *42* (3), 791–802.